

## Hydrophobic Effect in a Continuum Model of the Lipid Bilayer

Phillip L. Wilson<sup>1,\*</sup>, Huaxiong Huang<sup>2</sup> and Shu Takagi<sup>3</sup>

<sup>1</sup> *Department of Mathematics and Statistics, University of Canterbury, Private Bag 4800, Christchurch 8140, New Zealand.*

<sup>2</sup> *Department of Mathematics and Statistics, York University, Toronto, M3J 1P3, Canada.*

<sup>3</sup> *Department of Mechanical Engineering, The University of Tokyo, Tokyo, Japan.*

Received 16 August 2008; Accepted (in revised version) 24 December 2008

Available online 19 February 2009

---

**Abstract.** We study a continuum paradigm of the lipid bilayer based on minimizing the free energy of a mixture of water and lipid molecules. This paper extends previous work of Blom and Peletier [European J. Appl. Math., 15 (2004), pp. 487-508] in the following ways. (a) It formulates a more general model of the hydrophobic effect to facilitate connections with microscale simulations and first-principles analysis. (b) It clarifies the meaning and role of the model parameters. (c) It outlines a method for determining parameter values so that physically-realistic bilayer density profiles can be obtained, for example for use in macroscale simulations. Points (a)-(c) suggest that the model has potential to robustly connect some micro- and macroscale levels of multiscale blood flow simulations. The mathematical modelling in point (a) is based upon a consideration of the underlying physics of inter-molecular forces. The governing equations thus obtained are minimized by gradient flows via a novel numerical approach; this enables point (b). The numerical results are shown to behave physically in terms of the effect of background concentration, in contrast to the earlier model which is shown here to not display the expected behaviour. A “short-tail” approximation of the lipid molecules also gives an analytical tool which yields critical values of some parameters under certain conditions. Point (c) involves the first quantitative comparison of the numerical data with physical experimental results.

**AMS subject classifications:** 74G15, 74G65, 74K15, 74L15

**Key words:** Lipid bilayer, free energy, continuum model, numerical minimization.

---

\*Corresponding author. *Email addresses:* p.wilson@math.canterbury.ac.nz (P. L. Wilson), hhuang@mathstat.yorku.ca (H. Huang), takagi@mech.t.u-tokyo.ac.jp (S. Takagi)

## 1 Introduction

We show that a continuum paradigm [1] of the lipid bilayer can produce physically-realistic bilayer properties. We first introduce into the paradigm a new model of the hydrophobic effect. Secondly, we investigate the influence and meaning of the paradigm's parameters by performing the first quantitative comparison of numerical solutions of the paradigm with physical experimental data, and in so doing provide a method for determining parameter values.

As is well-known, the cell is the fundamental element of all living matter. The activity of the cell sustains life and the cell itself is sustained by a metabolism which utilizes mass transfer through its membrane. The cell membrane is composed of a double layer of lipid molecules (lipids) with proteins and other components floating in it [9]. The dynamics of this lipid bilayer membrane become especially important in the case of dispersed components in the blood, such as red blood cells (RBCs), white blood cells, platelets and so on, because the deformation dynamics of these membranes directly affect the mass transfer in the blood. These membranes are often modelled as hyperelastic due to the presence of a cytoskeleton. On the other hand, a liposome, composed of lipid bilayers only, is usually modelled as a two-dimensional fluid membrane, because the membrane lipid molecules can easily move laterally within the bilayer. Liposomes are used as drug delivery agents (DDAs) and artificial oxygen-carriers in blood. Although fluid, a "soft" entropic force called the hydrophobic force (or effect) gives the pure lipid bilayer integrity [3].

In all these cases the behavior of the lipid bilayer is responsible for the mass transfer through the cell membranes. Hence, the modelling of the lipid bilayer membrane from a molecular level through to the continuum level is expected ultimately to predict mass transfer behavior in blood [2, 8, 10, 11].

Here we focus on one crucial intermediate scale the mesoscale at which both molecular physics and continuum mechanics are important to the bilayer dynamics, since the bilayer is typically only two molecules in thickness but extends laterally for several micrometers. Understanding how membrane composition affects deformability, and how deformation affects the mass-transfer properties of RBCs and DDAs, are key to the multiscale modelling of blood flow. In this paper, we consider bilayers composed of one type of lipid.

[1] base their continuum paradigm, herein called the "BP paradigm", on the mesoscopic dynamics framework of [5], minimizing a free energy for a system of lipid and water molecules. Formally, the intrinsic free energy of the system is minimized with respect to a constraint that the (unobservable) distribution of the molecules generates the (observable) continuous volume fractions, thus assuming that the microstate has relaxed to equilibrium over the relatively long time scale of the continuous description.

Within this paradigm, several different models of lipid structure and inter-molecular interaction may be considered, and here we present a new interaction model which differs from the original choice in [1] in a number of ways. Our main point is a new model of the hydrophobic effect which has two advantages over the original, both stemming from

the fact that our model deals with physical attractive forces between molecules. Thus, on the one hand, the model is more general than the original which penalized proximity between waters and tails, whereas the new model promotes the hydrogen-bond network in which heads and waters partake, making the appearance of bilayer-like solutions less obvious. On the other hand, by working with attractive inter-molecular forces we feel that our model is more physical and anticipate being able to connect the model more readily with microscale simulations, and also with first-principles analysis.

A further improvement supporting the above advantages is a term  $\beta$  to control the decay rate of the interaction strengths. Since tests not reported here show that both models have very similar computational costs, we concentrate largely on our new model. Our point is not that our model has computational advantages or performs better under certain conditions, but rather that it is more general and more physical, enabling a better connection to microscale simulations or first principles. Moreover, although [1] demonstrated that the paradigm in principle has bilayer-like solutions, we are able to show that further that, with our model, the paradigm actually generates bilayer profiles with physically-realistic properties which can be fine-tuned to create model bilayers for different lipid species. It does so while yet being relatively fast to solve numerically, and relatively straight-forward to analyze, lending credibility to the numerical solutions.

Our analysis of the paradigm shows that some of its parameters which at first sight appear physical (as opposed to purely numerical) are in fact largely numerical, in that they cannot be directly connected *a priori* with physical measurements. Properties of numerical bilayers must be compared *a posteriori* with physical properties in order to set some parameter values. The numerical bilayers are obtained by a method of solution new to the paradigm, and are for the first time quantitatively compared with experimental measurements of physical bilayers, and fine-tuned to match them.

In more detail, the system of water molecules and heads and tails of lipids has a free energy split into an ideal part roughly corresponding to the Helmholtz free energy, involving only connectivity interactions, and a non-ideal part representing inter-molecular interactions. Lipid structure and configuration are therefore explicitly represented. [1] formulate a non-ideal part of the free energy with a term reflecting the (global) compressibility of the system and another modelling the (local) hydrophobic interactions; the modelling of the hydrophobic interaction term is an open question and is not inherent to the formalism of [5]. In this paper we introduce a new model of the hydrophobic interactions which captures the physics underlying the hydrophobic effect, based on the following discussion.

Liquid water is a dynamic hydrogen bond network in which each water molecule forms up to four hydrogen bonds with its neighbours. The non-zero dipole moment of lipid head groups makes them able to accept hydrogen bonds from water molecules (but unable to donate a bond to each other): they are hydrophilic. By contrast, the hydrophobic lipid tail groups are unable to form hydrogen bonds, although thermodynamic and electrostatic interactions between water molecules and tail groups occur, but in liquid water at room temperature the hydrogen-bond energy is typically an order of magnitude

stronger than such interactions [6,9].

A cavity with a structured “surface” in the hydrogen bond network forms around a hydrophobic moiety, causing a decrease in the entropy of the system [7]. An entropic “force” acts to gather together hydrophobic moieties so as to minimize the disruption to the hydrogen bond network. The physical origin of this hydrophobic effect is that water molecules close to a sufficiently large hydrophobic moiety no longer participate in four hydrogen bonds; with no attractive force towards the hydrophobic moiety, these molecules’ remaining bonds now draw them away from the moiety. It is thus because lipid head groups can be nodes in the hydrogen bond network while tail groups cannot that bilayers and other structured lipid assemblies form, and this is the basis of our model.

Of the physical parameters, we take the system to be incompressible, leaving the effects of the compressibility parameter  $p$  to future work. The relative tendency of heads and waters to form hydrogen bonds is modelled here by the new parameter  $\gamma$  which is set as unity in this paper: the effects of  $\gamma$  are also left to future work, while we simply note here that  $\gamma$  moves the paradigm beyond modelling heads as attached water molecules. Herein we investigate the effects of the key physical parameters  $\alpha, \epsilon, \beta, c_0$ , and  $m$ . Respectively these represent temperature effects, lipid head-tail group separation distance, decay of the interaction strength, and a “background concentration” and “excess mass” of lipids (these last two terms, inherited from [1], are clarified in this paper).

The paper is structured as follows. We introduce into the BP paradigm a new model of the inter-molecular interactions in Section 2.1 which forms the basis of the numerical solutions. The parameters and lipid model are discussed here. Euler-Lagrange equations, whose solution minimizes the free energy functional, are derived in Section 2.2, and a novel numerical approach to solving them is given in Section 2.3, along with a sample numerical result. All solutions and discussions are based on a one-dimensional model. The “smoothed” nature of the paradigm and the choice of lipid model are discussed in Section 2.4.

Section 3 connects the BP paradigm to physical *in vitro* measurements of lipid bilayers. The summary of bilayer properties in Section 3.1 is used in Section 3.2 to describe how numerical solutions can be calibrated to physical data. Numerical solutions are calibrated in this way for the parameters of interest in Section 3.2.1,2,3. In particular, a short-range interaction (or “short-tail”) approximation based on the new parameter  $\beta$  is introduced in Section 3.2.2, and its effects studied analytically and numerically. This work enables guidelines on the choice of parameter values to be given in Section 3.3. The conclusions are in Section 4.

## 2 The new model: derivation and numerics

### 2.1 The new model

The original model of the hydrophobic interaction acted to move tails away from heads and waters by penalizing proximity between them, mimicking the *effect* of the hydropho-

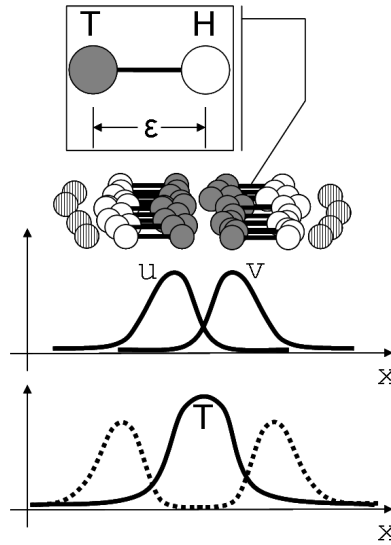


Figure 1: Cartoon of the setup, showing the basic lipid structure, the key parameter  $\epsilon$ , the direction  $x$  normal to the plane of the bilayer, and the water molecules represented by hatched circles. Below is drawn a sketch of the densities of the two tail groups  $u$  and  $v$ , from which are extracted the total tail density  $u+v$  (solid line), and total head density  $\tau_{-\epsilon}u + \tau_{\epsilon}v$  (dashed line).

bic force but not the underlying *cause*, which ultimately rests on the attractive forces of the hydrogen bond network. Our approach, in direct contrast to the original model, is to promote water-water and water-head (but not head-head) proximity, modelling the hydrogen bond network, and effectively to ignore the hydrophobic tails. The relative strength of the water-water bonding preference to the water-head bonding preference is controlled by a parameter  $\gamma$ .

Formally, our system comprises “waters”, each represented by a single “bead”, and “lipids”, each represented by a “head” bead and a “tail” bead<sup>†</sup> connected by a rigid massless rod of length  $\epsilon$ . The one-dimensional model has two lipid groups aligned in the  $x$ -direction, normal to the bilayer plane, as illustrated in Fig. 1. One group has tails, having normalized density  $u(x)$ , pointing in the positive  $x$ -direction, and the other has tails of normalized density  $v(x)$  pointing in the negative  $x$ -direction. The head beads of the first group have normalized density  $\tau_{-\epsilon}u(x) = u(x+\epsilon)$ , and similarly for the second. Water beads have normalized density  $w(x)$ . The lipids have here been chosen as the simplest allowed in the paradigm; see Section 2.4.

The total free energy of the system consists of three parts in the form

$$E = T \int [\eta(u) + \eta(v) + \eta(w)] dx + \frac{p}{2} \int (1 - u - v - \tau_{-\epsilon}u - \tau_{\epsilon}v - w)^2 dx + \alpha \int w \hat{\kappa} * [w + \gamma(\tau_{-\epsilon}u + \tau_{\epsilon}v)] dx. \quad (2.1)$$

<sup>†</sup>All beads are of zero dimension.

The integration measure is the spatial dimension  $x$ . In real terms this would run between the two sides of the container holding the lipid-water mixture — effectively  $\pm\infty$  on the working length scale. In practice, we integrate numerically over a domain periodic modulo  $2L$ , for some  $L \gg \epsilon$ . The new model differs from the original in the third integral; the meanings of all three integrals, and the parameters and variables follow.

The first integral, favouring spreading, represents the entropy of the system, in which  $\eta(s) = s \log s$  for non-negative  $s$  and  $\eta(s) = \infty$  otherwise, and where  $T$  is the temperature of the system. The second integral is a potential energy due to compressibility, where  $p$  is the system pressure.

The third integral involves a water-water term  $w\hat{\kappa}*w$  and a water-head term  $w\hat{\kappa}*\gamma(\tau_{-\epsilon}u + \tau_{\epsilon}v)$ , where  $*$  indicates convolution in the form

$$(f\hat{\kappa}*g)(x) = \int f(x)\hat{\kappa}(x-y)g(y) dy. \quad (2.2)$$

The overall strength of these interactions is controlled by  $\alpha$  with their relative strength controlled by  $\gamma$ .

The convolution measures the extent to which members of the two bead types represented by  $f$  and  $g$  in (2.2) are in proximity at a given point. For example, the term  $w\hat{\kappa}*\gamma(\tau_{-\epsilon}u + \tau_{\epsilon}v)$  is a function of  $x$  and effectively measures the proximity between water beads at  $x$  and head beads in the rest of the domain of integration. Although we take the opposite approach, the kernel function  $\hat{\kappa}$  can be chosen to “penalize” proximity between the bead types by producing a large contribution to the energy functional when aggregation occurs; since we seek to minimise the energy functional, the solution moves away from this situation. By contrast we “reward” proximity by taking the interaction kernel to be

$$\hat{\kappa}(s) = \kappa_0 - \kappa(s) \quad \text{for} \quad \kappa(s) = \delta_{\beta}(s), \quad (2.3)$$

where  $\delta_{\beta}(s)$  is a general smooth function with the properties

$$\delta_{\beta}(\pm\infty) = 0, \quad \int \delta_{\beta} dx = 1,$$

and the constant  $\kappa_0$  is chosen so that  $\int \hat{\kappa} dx = 1$ . In this paper, we define

$$\hat{\kappa}(s) = \kappa_0 - \frac{1}{2\beta} e^{-|s|/\beta}, \quad (2.4)$$

although other choices could be considered. The new kernel  $\hat{\kappa}(s)$  rewards proximity and thus represents an attractive water-water and water-head force, in contrast to the original model of [1] which penalized water-tail and head-tail proximity. The new parameter  $\beta$  controls the decay of the hydrophobic interaction, and will be shown in Section 3.2.2 to introduce a straightforward analytical tool.

The system is taken to be infinite with an averaged density  $c_0$  for both  $u$  and  $v$ . To simplify the analysis and computation we consider the case of periodic cells of length  $2L$ ,  $L \gg \epsilon$ . All the discussions are valid for the infinite system.

## 2.2 Derivation of the Euler-Lagrange equations

Here we take the system to be incompressible,  $p = \infty$ , so that

$$1 - u - v - \tau_{-\epsilon}u - \tau_{\epsilon}v - w = 0. \quad (2.5)$$

The energy functional can be simplified as

$$E_I = \int [\eta(u) + \eta(v)] dx + \alpha \int (1 - u - v - \tau_{-\epsilon}u - \tau_{\epsilon}v) \hat{\kappa} * (1 - u - v) dx \quad (2.6)$$

subject to constraints

$$\text{non-negative water density} \quad 1 - u - v - \tau_{-\epsilon}u - \tau_{\epsilon}v = w \geq 0, \quad (2.7a)$$

$$\text{mass conservation} \quad \int (u + v - 2c_0) dx = m. \quad (2.7b)$$

The result of scaling  $T$  into  $\alpha$  is that we can consider the temperature effects by varying  $\alpha$ ; see Section 3.2.3. We have also dropped the entropy of the water molecules, which is justified since although the entropy changes of the water associated with reduced configurational arrangements around hydrophobic moieties actually assists solvation, the effect is very small [7]. Furthermore, we have taken  $\gamma = 1$ , effectively indicating that the electronegativities of waters and heads are equal, and leaving the effects of the relative strength of the water-water to water-head bonding preference to future work.

Using the definition (2.4) of the interaction kernel and the mass conservation constraint (2.7b) the energy functional becomes

$$E_I = \int [\eta(u) + \eta(v)] dx + \alpha \left( 1 - 2c_0 - \frac{m}{2L} \right) \int (1 - u - v - \tau_{-\epsilon}u - \tau_{\epsilon}v) dx - \alpha \int (1 - u - v - \tau_{-\epsilon}u - \tau_{\epsilon}v) \kappa * (1 - u - v) dx, \quad (2.8)$$

where we have chosen  $\kappa_0 = (2 - e^{-L/\beta})/2L$ . Using the method of Lagrange multipliers we rewrite the energy functional as

$$E_T = E_I + \frac{K}{2} \int \mu^2 dx + \lambda_+ \left( m - \int u + v - 2c_0 dx \right) + \lambda_- \left( \int u + v - 2c_0 dx - m \right), \quad (2.9)$$

where  $K$  and  $\lambda_{\pm}$  are Lagrange multipliers and  $\mu = (u + v + \tau_{-\epsilon}u + \tau_{\epsilon}v - 1)_+$ , with  $(\cdot)_+ = \max\{\cdot, 0\}$ .

Carrying out calculus of variations in a formal way, assuming that the order of integrations and translations can be changed wherever necessary, we derive the Euler-Lagrange equations

$$0 = \log u - \alpha \kappa * (2u + 2v + 2\tau_{-\epsilon}u + \tau_{-\epsilon}v + \tau_{\epsilon}v) + K\mu + K\mu(x + \epsilon) + \lambda, \quad (2.10a)$$

$$0 = \log v - \alpha \kappa * (2u + 2v + \tau_{-\epsilon}u + \tau_{\epsilon}u + 2\tau_{\epsilon}v) + K\mu + K\mu(x - \epsilon) + \lambda, \quad (2.10b)$$

where

$$\lambda = \lambda_- - \lambda_+ + 1 + 3\alpha - 2\alpha(1 - 2c_0 - m/2L). \quad (2.11)$$

We solve the Euler-Lagrange equations by first replacing them with evolution equations based on gradient flows:

$$u_t = -\log u + \alpha\kappa*(2u + 2v + 2\tau_{-\epsilon}u + \tau_{-\epsilon}v + \tau_{\epsilon}v) - K\mu - K\mu(x + \epsilon) - \lambda, \quad (2.12a)$$

$$v_t = -\log v + \alpha\kappa*(2u + 2v + \tau_{-\epsilon}u + \tau_{\epsilon}u + 2\tau_{\epsilon}v) - K\mu - K\mu(x - \epsilon) - \lambda, \quad (2.12b)$$

for the gradients  $u_t = -(\delta E / \delta u)$ ,  $v_t = -(\delta E / \delta v)$ , with given values of  $K, \lambda$ . These equations are solved numerically in the next section.

There are thus nine model parameters in total: seven apparently physical and two ( $K, \lambda$ ) strictly numerical.  $K$  and  $\lambda$  will be chosen subject to stability, symmetry, and water conservation considerations described shortly. Of the physical parameters we consider herein  $\epsilon, \beta, c_0, m, \alpha$ , as described previously.

### 2.3 Numerical scheme and solutions

Our numerical scheme solves the gradient flow equations (2.12a,b) to find the densities  $u, v$  which minimize the Euler-Lagrange equations (2.10a,b). The approach uses a discretized grid with finite difference formulae for  $u_t, v_t$ . Both first- and second-order backward differencing was used, with the results in close agreement. Generally, very small time steps were required. The numerical domain was taken to be periodic and of length  $2L$ , in contrast to [1] who used a finite domain with small decay at the edges. In both approaches,  $u, v$  deviate from  $c_0$  at the boundaries. In tests using the original model, our numerical scheme reproduced the profiles of [1], as near as we can tell, given that their simulation conditions were not fully specified. Typical runtime on a machine with two 2GHz AMD Opteron 270 Dual Core processors with 16GB of DDRS-667 SDRAM is four minutes.

The values of the Lagrange multipliers  $K, \lambda$  are not specified by the model. Indeed, we require an explicit penalty term in the algorithm, effectively replacing  $\lambda_- - \lambda_+$  in  $\lambda$  with  $\lambda^*(\int u + v - 2c_0 dx - m)$ . Within the range of values of  $K, \lambda^*$  for which the numerics are stable,  $K$  is chosen large enough to ensure  $w \geq 0$  but no larger, and  $\lambda^*$  is chosen to ensure that the solutions are symmetrical, as expected. Typically,  $K$  is of the order of  $10^3$  (but can be as large as  $\mathcal{O}(10^4)$ ), whereas  $\lambda^*$  is around  $10^2$ .

A sample result is shown in Fig. 2. The system has separated into a well-defined bilayer-like profile, in which the hydrophobic tail region is separated from the water region by two peaks in the hydrophilic head group density. Although it is not our purpose to compare solutions of our model with those of the original model of [1], we here note briefly that the forms are similar, but with lipids being slightly more strongly drawn into the bilayer of the new model. All the results presented in this paper are independent of domain length  $2L$  (above a certain value) and grid resolution (beyond some level of coarseness).

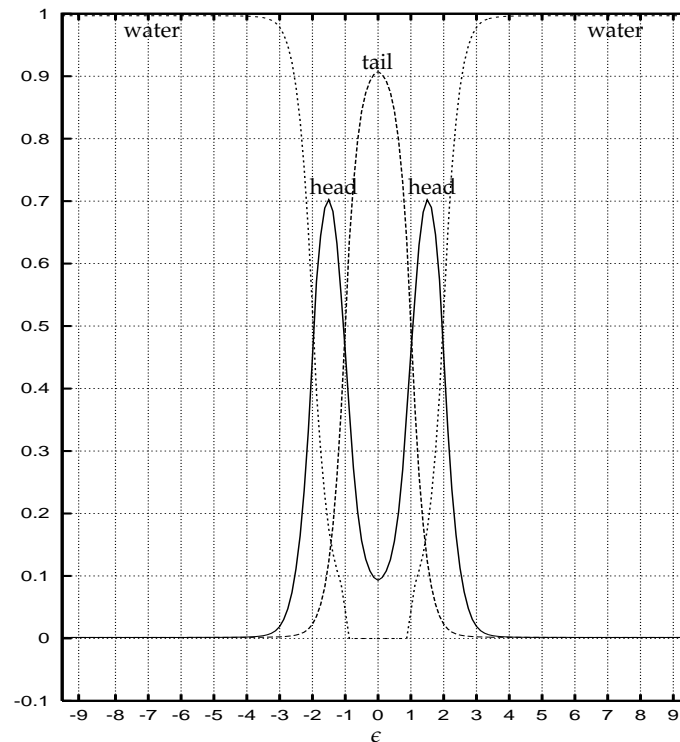


Figure 2: A sample “bilayer” for the parameter set  $\alpha=3, \epsilon=2, \beta=1, c_0=0.024, m=0.05*2L$ .

## 2.4 Smoothing and the choice of lipid model

There is no one-to-one correspondence between the paradigm’s “lipids” and the physical lipid molecules, but there is a rigorous correspondence between the densities of the one and those of the other. We prefer to call the paradigm’s “lipid” a *model lipid component*. These components represent as-yet unclear spatial and temporal smoothing of the molecular-level information. The temporal smoothing, is central to the paradigm and is important not just because it enables access to longer time scales, but also because it captures some detail of the real thermal motion of the lipid molecules within the bilayer, which is a defining characteristic of bilayers and plays a key role in their function. Regardless, we are free to choose any lipid component model; we have here picked the simplest. All information from the physical lipid is smoothed into (some sum of the densities of) the two beads, capturing *all* of the molecular data in a smaller number of variables.

Together, the spatial and temporal smoothing is evident in the numerical results since the model lipid components have combined to create a bilayer of total width greater than the naively-expected  $2\epsilon$ , as can be seen in Fig. 2 (see a more formal discussion in Section 3.2).

### 3 Connecting the paradigm with the physics

#### 3.1 Physical bilayer properties

Three biologically significant membrane characteristics are (1) the elastic moduli, (2) the intrinsic monolayer curvature, and (3) the bilayer thickness [9]. The latter is the focus of the present section ((1) and (2) require working in higher dimensions).

The averaged thickness  $d_{SZ}$  of the hydrophobic core, or saturation zone where  $w \approx 0$ , is a common physical measure of bilayer thickness. In a physical system this can be increased by the following means [9, §8.3]: increasing the length  $l_T$  of the tails; replacing the double carbon bonds by single bonds in the tails; decreasing the degree of hydration; increasing the cholesterol concentration; decreasing the temperature. These effects can increase  $d_{SZ}$  by several percent [9, Section 9.2].

The main approaches used in physical experiments to determine the time-averaged structure of lipid bilayers, and hence their thickness, exploit the high structural periodicity in the  $x$ -direction normal to the bilayer, for example in combining diffraction data from x-ray and neutron scattering [12]. One such data set is represented in Fig. 3 for the DOPC lipid molecule. In this figure, the water density measures only the waters of hydration (those bonded to head groups).

#### 3.2 Making comparisons with physical measurements

For our analysis the key features of Fig. 3 are the saturation zone, the density curves of the end of the tails (here, the  $CH_3$  moiety of DOPC), and those of the heads (here, choline and phosphate). The DOPC bilayer will form the basis of the comparative work in this paper, but the key point is that any single-species bilayer can be simulated by our model within the BP paradigm, when basic structural details are known from experiments.

We consider only those numerical results with a clear bilayer structure like that of Fig. 2, namely with a single saturation zone of width  $d_{SZ}$ , a single tail peak with exactly two transitions from concavity to convexity, and two head peaks of equal width  $d_{HZ}$ , each likewise with exactly two transitions from concavity to convexity. The head zone width  $d_{HZ}$  is defined in the following way. Using the left-hand head peak, let  $x_L, x_R$  be the first points to the left and right of the peak satisfying  $h_x = 0, h_{xx} > 0$ , *i.e.* local minima, with the local maxima of the head peak located at  $x^*$ . We then find  $x_1, x_2$  from  $h(x_{1,2}) = \frac{1}{2}(h(x_{L,R}) + h(x^*))$  and define  $d_{HZ} = x_2 - x_1$ . Defining the head zone width in this way as running from the left-hand midpoint to the right-hand midpoint of the peak is not unusual (*e.g.* [9, fig 8.1]), but none of our conclusions is changed significantly by defining it as  $x_R - x_L$ .

In a physical system, the ratio  $d_{HZ}/d_{SZ}$  depends on the choice of lipid molecule (other factors such as temperature being equal) and so characterizes the bilayer properties for our purposes. For the DOPC bilayer of Fig. 3,  $d_{HZ}/d_{SZ} \approx 0.4$ .

We now show that varying the key paradigm parameters of Section 2.1 enables a so-

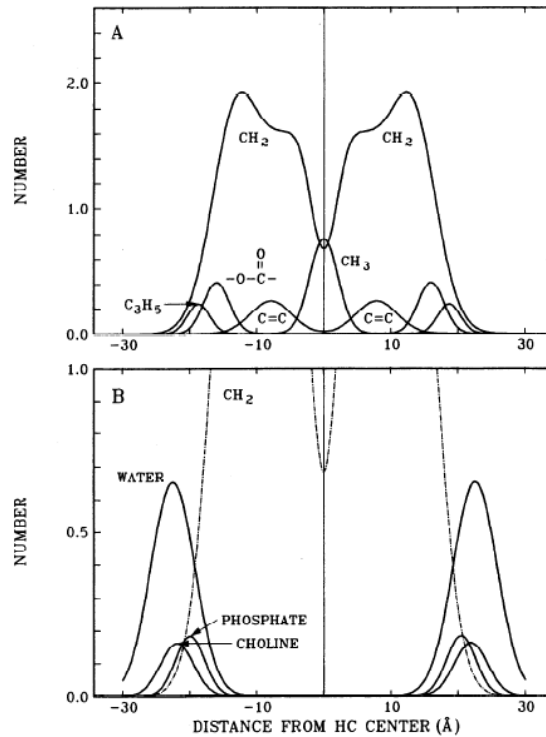


Figure 3: The experimentally-determined structure of a DOPC bilayer (figure reproduced from [12] with kind permission of the authors and the Biophysical Society).

lution to be found corresponding closely to any desired physical bilayer, with the DOPC bilayer as our example. The method of selecting the values of the parameters is summarized in Section 3.3.

### 3.2.1 $c_0$ , $m$ and the critical micelle concentration

The parameters  $c_0$  and  $m$  combine to form a numerical equivalent of the critical micelle concentration (CMC), in which the monomer density of lipids in solution only increases up to the CMC, beyond which the excess lipids aggregate into ordered structures. The CMC refers to an average lipid density, which here is

$$\bar{\rho} = \frac{2}{2L} \int u + v = \frac{m}{L} + 4c_0. \quad (3.1)$$

Consequently, the true background density is not  $c_0$  but  $m/L + 4c_0^*$ , where  $c_0^*$  is the value of  $c_0$  for which aggregates first form (with all other parameters fixed), and the total excess of lipids is  $8L(c_0 - c_0^*)$ . We numerically fix  $m$  at a working value and vary  $c_0$  only.

In Fig. 4 we consider three data sets in which the parameters  $\alpha$ ,  $\epsilon$ , and  $c_0$  vary, the values of  $\alpha$  and  $\epsilon$  being given in parentheses on the graph. The widths  $d_{HZ}$  and  $d_{SZ}$  are

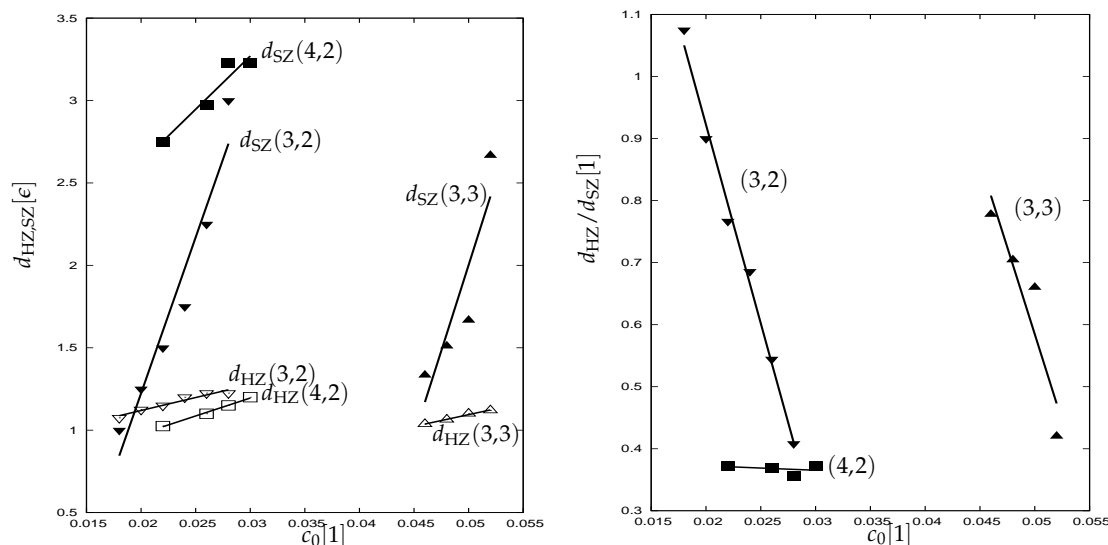


Figure 4: Top:  $d_{\text{HZ}}$  and  $d_{\text{SZ}}$  against  $c_0$  for three different pairs  $(\alpha, \epsilon)$ , with all other parameters equal. Bottom: the ratio  $d_{\text{HZ}}/d_{\text{SZ}}$  for the three parameter sets. Straight lines of best fit have been drawn.

normalized on  $\epsilon$  in these figures. Numerical data is represented by points and a straight line of best fit is drawn in each case.

As  $c_0$  increases beyond  $c_0^*$ , the excess lipids should be drawn into the bilayer with the numerical background concentration remaining more or less the same. This required increase of  $d_{\text{HZ}}$  and  $d_{\text{SZ}}$  with increasing  $c_0$  can be seen in the upper figure. It is worth noting here that the original model does not show the expected increase of  $d_{\text{HZ}}$  with  $c_0$ : indeed, an inverse relationship between  $d_{\text{HZ}}$  and  $c_0$  holds for numerical data generated by the original model, as shown in Fig. 5.

More importantly, the data from our new model can be combined into the ratio  $d_{\text{HZ}}/d_{\text{SZ}}$  as shown in the lower figure of Fig. 4. Taking the example of a DOPC bilayer, the data shows that we can choose suitable parameter sets such that  $d_{\text{HZ}}/d_{\text{SZ}} \approx 0.4$ , namely  $(\alpha, \epsilon, c_0) = (3, 2, 0.028)$  for which  $d_{\text{HZ}}/d_{\text{SZ}} = 0.41$ ,  $(\alpha, \epsilon, c_0) = (4, 2, 0.022)$  for which  $d_{\text{HZ}}/d_{\text{SZ}} = 0.37$ , and  $(\alpha, \epsilon, c_0) = (3, 3, 0.052)$  for which  $d_{\text{HZ}}/d_{\text{SZ}} = 0.42$ . We expect that ultimately  $\alpha$  can be set physically (see also Section 3.2.3) and that the role of  $\epsilon$  is more one of clarifying the structure (Section 3.2.2), so that effectively here our only choice would be  $c_0$ , and the data shows that a value can be chosen which yields a bilayer characteristic close to that desired. There is no apparent reason for this not to hold for lipids other than DOPC.

### 3.2.2 $\epsilon$ and the interaction decay length, $\beta$

That  $\epsilon$  is not an actual lipid length has already been discussed. Varying  $\epsilon$  changes the degree of separation of the head and tail regions, larger  $\epsilon$  giving clearer bilayer structure, meaning that we need only consider a few order unity values of  $\epsilon$ ; see also Section 3.3.

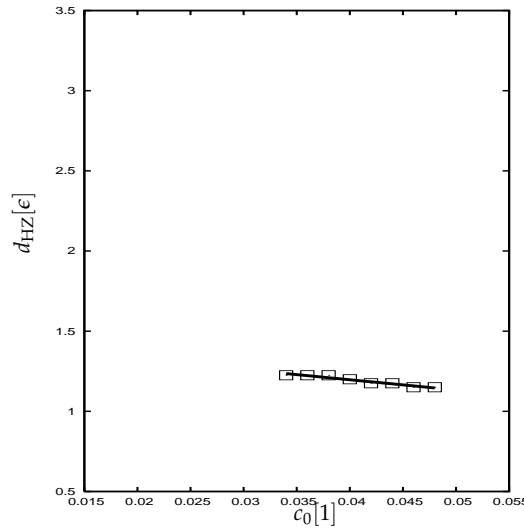


Figure 5: Example data for the original model:  $d_{\text{HZ}}$  against  $c_0$  for  $(\alpha, \epsilon) = (4, 2)$ , plotted on the same scale as figure 4. A straight line of best fit has been drawn, indicating a non-physical inverse relationship between  $d_{\text{HZ}}$  and  $c_0$ .

Turning to the parameter  $\beta$ , which controls the interaction decay length, we consider another special case of the kernel function of equation (2.4). Our “short-range interaction” approximation takes  $\beta \rightarrow 0$ , so that the kernel function approaches the delta function

$$\kappa(s) = \begin{cases} 1, & s = 0; \\ 0, & s \neq 0. \end{cases} \tag{3.2}$$

Taking also  $K \rightarrow \infty$ , the Euler-Lagrange equations (2.10) reduce to

$$\log u - \alpha(2u + 2v + 2\tau_{-\epsilon}u + \tau_{\epsilon}v + \tau_{\epsilon}v) = -\lambda, \tag{3.3a}$$

$$\log v - \alpha(2u + 2v + \tau_{-\epsilon}u + \tau_{\epsilon}u + 2\tau_{\epsilon}v) = -\lambda. \tag{3.3b}$$

Separating  $\lambda$  into a constant term plus a term dependent on  $c$  by rewriting (2.11) as  $\lambda = \bar{\lambda} + 2\alpha(2c_0 + m/2L)$ , we look for constant solutions  $u = v = c$ , obtaining

$$\log c - 4\alpha c = -\bar{\lambda}. \tag{3.4}$$

Differentiating (3.4) with respect to  $c$  yields the critical concentration  $c_c$  as the first necessary condition for the existence of a solution:

$$c = c_c \equiv \frac{1}{4\alpha}. \tag{3.5}$$

The short-range interaction tool thus gives a simpler way to find the same result (3.5) as [1]. To simplify our discussion, we assume that  $c_0 = c_c = 1/4\alpha$  and take  $\alpha \geq 1$ .

The other necessary condition for the existence of a solution is estimated as follows. From the incompressibility condition (2.7a) we see that  $c \leq 0.5$ . Substituting  $c = 0.5$  into (3.4) gives

$$\bar{\lambda}_{\min} = -\log 2 - 2\alpha. \quad (3.6)$$

When there is phase separation, (3.4) must have more than one solution: indeed,  $\bar{\lambda}$  must also be less than  $\bar{\lambda}_{\max}$  where

$$\bar{\lambda}_{\max} = \log c_c - 4\alpha c_c = -\log(4\alpha) - 1, \quad (3.7)$$

in which case there is only one solution. When  $\beta = 0$  the incompressibility condition implies  $c \leq 0.25$ , and therefore

$$\bar{\lambda}_{\min} = -\log 4 - \alpha. \quad (3.8)$$

With  $\bar{\lambda}_{\min} < \bar{\lambda} < \bar{\lambda}_{\max}$  there are many possible states. The relevant question is whether there exists a global minimum of the  $\delta$ -function free energy

$$E_D = \lim_{\beta \rightarrow 0} E_I = \int \eta(u) + \eta(v) + \alpha \left( u + v - 2c_0 - \frac{m}{L} \right) (1 - u - v - \tau_{-\epsilon} u - \tau_{\epsilon} v) dx. \quad (3.9)$$

With  $\bar{\lambda}$  chosen between its minimum and maximum values, we assume that  $u = v = c_1$  for  $-l < x < l$ , some  $l < L$ , and  $u = v = c_2$  elsewhere, where  $c_1$  and  $c_2$  are two distinct solutions of (3.4). The mass conservation (2.7b) gives

$$l = \frac{m + 4L(c_0 - c_2)}{4(c_1 - c_2)}, \quad (3.10)$$

which in (3.9) yields

$$\begin{aligned} \frac{E_D}{4} = & l \left[ c_1 \log c_1 - c_2 \log c_2 + 2\alpha \left( 2(c_1 + c_2) + 2c_0 + \frac{m}{L} \right) (c_1 - c_2) \right] \\ & + L \left[ c_2 \log c_2 + \alpha \left( c_0 + \frac{m}{2L} \right) (4c_2 - 1) + 4\alpha c_2^2 \right] - \epsilon \alpha (c_1 - c_2)^2. \end{aligned} \quad (3.11)$$

In Fig. 6, we have plotted  $E_D$  as a function of  $\bar{\lambda}$ , for  $(\alpha, \epsilon) = (4, 2)$ . We can see that the global minimum occurs when  $\bar{\lambda} = \bar{\lambda}_{\max}$ .

Returning to the question of finding a desired profile, Fig. 7 shows how  $d_{\text{HZ}}, d_{\text{SZ}}$  and their ratio vary with  $\beta$  for all other parameters fixed. A multi-lammellar profile began to appear for  $\beta < 0.75$ , while separation without a saturation zone appeared for  $\beta > 2.25$ . Crucially, a bilayer-like profile could be found for all values of  $\beta$  in the given range, meaning that, by varying  $\beta$ , the important ratio  $d_{\text{HZ}}/d_{\text{SZ}}$  can be fine-tuned to the desired accuracy; see Section 3.3.

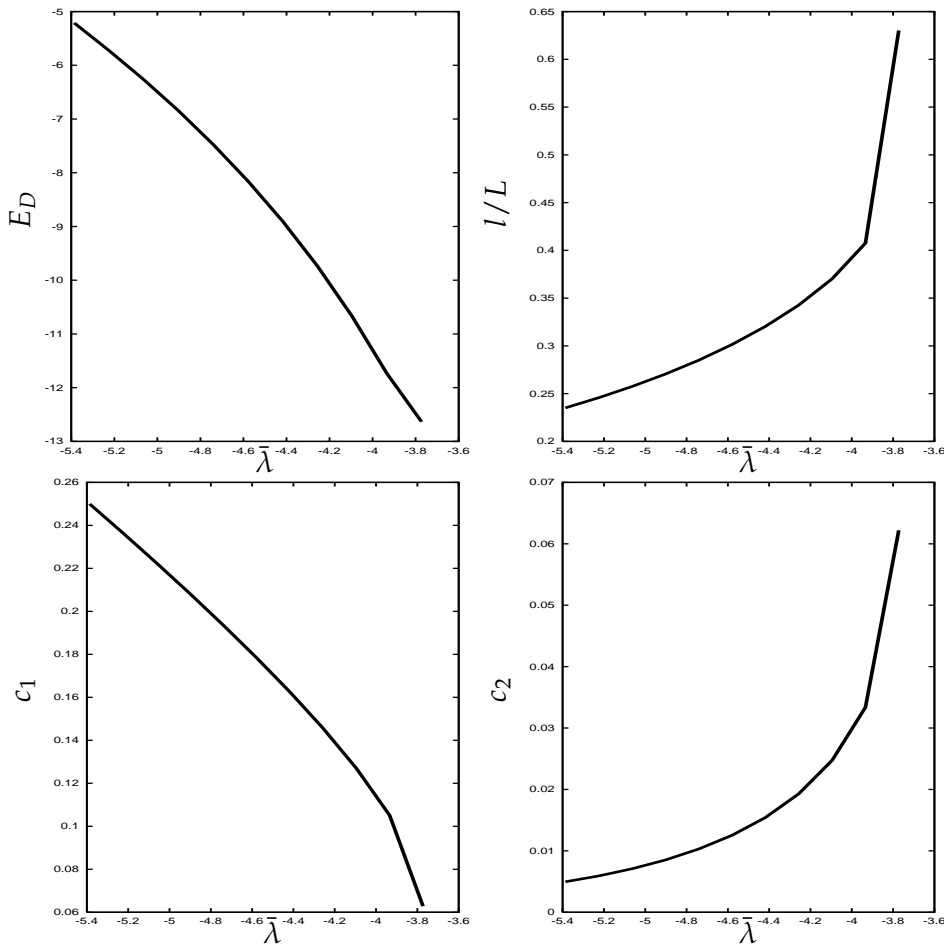


Figure 6: Solutions of Eqs. (3.11), (3.10), (3.4) for the parameters  $\alpha=4, \epsilon=2, c_0=1/(4\alpha), m=c_0/10, L=20$ .

### 3.2.3 $\alpha$ and the effects of temperature

With reference to Section 3.1, increasing  $\alpha$  should increase the measurable  $d_{SZ}$ . Because this can be seen in Fig. 4, it appears that temperature-related mechanisms can be captured in 1D. Indeed, turning to the incompressible free energy functional (2.6) in which  $\alpha$  is scaled on  $T$ , increasing  $\alpha$  (decreasing  $T$ ) reduces the effect of the entropy relative to the interaction terms. This makes physical sense in that with less kinetic energy the hydrogen-bond network is more strongly preserved.

Further, the other physical temperature-related mechanism is that by which lower temperatures straighten the lipid tails on average. As a result, we would expect the ratio  $d_{HZ}/d_{SZ}$  of our model to decrease as  $\alpha$  increases ( $T$  decreases), and this is seen in Fig. 4.

Finally, we note that if the model were also capturing thermal undulations then  $d_{SZ}$  would decrease as  $\alpha$  increased, because the order of magnitude of the thermal fluctua-

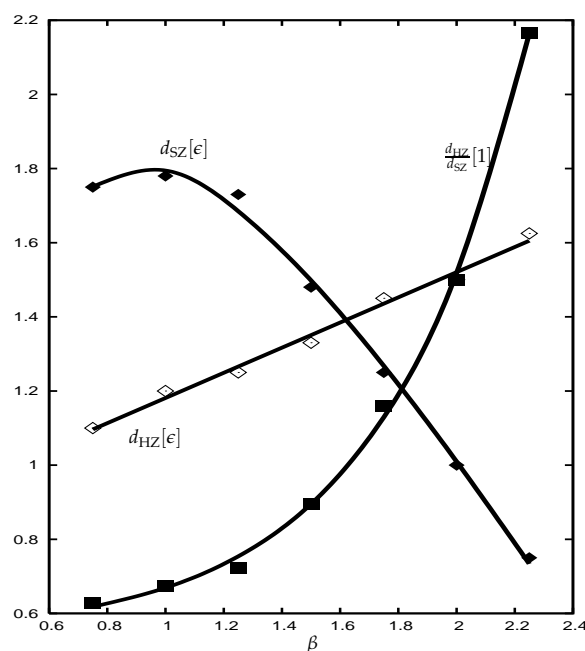


Figure 7:  $d_{\text{HZ}}$ ,  $d_{\text{SZ}}$ ,  $d_{\text{HZ}}/d_{\text{SZ}}$  for different values of  $\beta$ . The other parameters were fixed: in particular,  $(\alpha, \epsilon, c_0) = (3, 2, 0.024)$ . For  $d_{\text{HZ}}$  the drawn line of best fit is straight  $ax+c$ , for  $d_{\text{SZ}}$  it is of the form  $ax+b/x+c$ , and for the ratio it is exponential and of the form  $a\exp(bx)+c$ .

tions is larger than that of the changes in  $d_{\text{SZ}}$ . Since we see the opposite, this precludes using the amplitude of an averaged thermal undulation to fix  $\alpha$ .

### 3.3 Choosing a parameter set

Based on the preceding sections, we can set the parameters to reproduce the profile of a desired lipid species bilayer whose properties are known *a priori* from experimental data as follows.

Choose  $\alpha = 3$  or 4, noting from Fig. 4 that from the numerical viewpoint  $\alpha$  controls the sensitivity of the ratio  $d_{\text{HZ}}/d_{\text{SZ}}$  to variation in  $c_0$ . Then, pick  $\epsilon = 2$  or 3, essentially only requiring clear separation of the head and tail regions. Next set  $\beta = 1$  to start. Now run the numerics with several  $c_0$  until  $d_{\text{HZ}}/d_{\text{SZ}}$  is close to the desired value. Finally, fine-tune the results by varying  $\beta$ .

## 4 Conclusions

We introduced a more general model of the hydrophobic effect into the continuum paradigm of [1] and showed that one-dimensional numerical solutions can reproduce key characteristics of physical lipid bilayers. In particular, the mechanically-important

bilayer thickness can be reproduced. Indeed, various key characteristics were shown to behave physically, with at least one in contrast to an unphysical behaviour of the original model. The paradigm's inherent smoothing of the molecular information was discussed, and the smoothed numerical data calibrated to measurements of physical bilayers. Examining some of the key parameters in turn, we gave a strategy for setting their values, noting that future work, especially in higher dimensions, could make this process even more robust by further appeal to physical arguments. In particular,  $\alpha$  is formally linked to the temperature, and has been shown here to have a corresponding effect on the numerical results, while  $\beta$  should be related to the range of the hydrogen bonding forces. Already, however, the new parameter  $\beta$  has introduced the short-range interaction tool, allowing analytical results to be obtained with greater ease.

The main aim of future work is to consider higher dimensions, and include compressibility effects by allowing  $p$  to vary. If the conclusions of the current paper are supported by higher-dimensional work, then the paradigm can be made as physical as desired by varying  $\gamma$ , considering other  $\kappa$  (and indeed whether "promoting proximity" is the best model of the underlying physics), including electrostatic effects, weak head-head van der Waals repulsion terms, and so on. The level of detail will rest on computational issues, in particular cost-benefit considerations in the light of the paradigm's potential use as a mesoscale numerical filter in multiscale numerical simulations.

Extending the 1D model to higher dimensions represents a significant challenge. In one dimension, the lipids are all aligned and split into two distinct species. This is not true in higher dimensions. As a first step towards generalizing our 1D model to higher-dimensional cases, work is underway to develop a quasi-2D model which is computationally tractable. This model allows lipid density variations in 2D while restricting the lipid alignment to 1D. This approach would allow for the formation of 2D bilayers, but not for out-of-plane bending. A generalization, while yet remaining computationally tractable, would be to allow small-angle deviations from an aligned state. In this way, long wavelength, small amplitude bilayer fluctuations would be allowed. Moreover, this approach may permit the study of embedded protein aggregation and the influence this can have on vesiculation and membrane fusion [4]. We believe that this extension of the present model to 2D is more feasible than tackling the seven coupled integro-differential evolution equations forming a more complete model in [1].

## Acknowledgments

P.L.W. gratefully acknowledges the support of the Japan Society for the Promotion of Science and the University of Tokyo's Intelligent Modeling Laboratory during part of this work. His thanks for many helpful discussions go to members of the IKEMEN group of the Fluid Engineering Laboratory of the University of Tokyo. H.H. would like to acknowledge the support from JSPS through its fellowship program, and grants from NSERC and MITACS (Canada). We also thank the RIKEN institute for their sup-

port through the project Research Program for Computational Science, R&D Group for the Next-generation Integrated Simulation of Living Matters, which is supported by the Japanese Ministry of Education, Culture, Sports, Science and Technology.

## References

- [1] J. G. Blom and M. A. Peletier, A continuum model of lipid bilayers, *European J. Appl. Math.*, 15 (2004), 487-508.
- [2] K. Boryczko, W. Dzwinel and D. A. Yuen, Dynamical clustering of red blood cells in capillary vessels, *J. Mol. Model.*, 9 (2003), 16-33.
- [3] D. Chandler, Interfaces and the driving force of hydrophobic assembly, *Nature*, 437 (2005), 640-647.
- [4] L. V. Chernomordik and M. M. Kozlov, Mechanics of membrane fusion, *Nature Structural & Molecular Biology*, 15 (2008), 675-683.
- [5] J. G. E. M. Fraaije, Dynamic density functional theory for microphase separation kinetics of block copolymer melts, *J. Chem. Phys.*, 99 (1993), 9202-9212.
- [6] E. H. Immergut, *Encyclopedia of Applied Physics* vol. 18, V.C.H. Berlin, 1991.
- [7] B. Kronberg, M. Costas and R. Silveston, Thermodynamics of the hydrophobic effect in surfactant solutions — micellization and adsorption, *Pure & Appl. Chem.*, 67 (1995), 897-902.
- [8] G. Mchedlishvili and N. Maeda, Blood flow structure related to red cell flow: determination of blood fluidity in narrow microvessels, *Jpn J. Physiol.*, 51 (2001), 19-30.
- [9] O. G. Mouritsen, *Life - as a Matter of Fat*, Springer-Verlag Berlin, 2005.
- [10] T. Sugii, S. Takagi and Y. Matsumoto, A molecular-dynamics study of lipid bilayers: effects of the hydrocarbon chain length on permeability, *J. Chem. Phys.*, 123 (2005), 184714.
- [11] N. K. Vaidya, H. Huang and S. Takagi, Modelling HA protein-mediated interaction between an influenza virus and a healthy cell: pre-fusion membrane deformation, *Math. Med. Biol.*, 24 (2007), 251-270.
- [12] M. C. Wiener and S. H. White, Structure of a fluid dioleoylphosphatidylcholine bilayer determined by joint refinement of X-ray and neutron diffraction data, *Biophys. J.*, 61 (1992), 434-447.